Environmental Science & Technology

pubs.acs.org/est

Article

Fate of 1 to 6 nm Candle Combustion Nanoparticles in Indoor Atmospheric Environments

Satya S. Patra, Gerhard Steiner, and Brandon E. Boor*

Cite This: *Environ. Sci. Technol.* 2026, 60, 834−846

Read Online

ACCESS | Metrics & More | Article Recommendations | Supporting Information

ABSTRACT: Nano-organic carbon (NOC: 1−6 nm) particles are emitted during combustion processes and remain understudied down to their smallest sizes in indoor environments. We investigate the persistence of atmospheric nanoparticles in the NOC size range indoors during scented candle combustion in a residential test house. Our results indicate that atmospheric nanoparticles in the 1−6 nm size range dominate indoor particle concentrations, constituting up to ∼65% of total particles. The fate of these nanoparticles in indoor air is mainly governed by their apparent emission rates and the coagulation scavenging potential of the indoor atmosphere, parametrized through the net coagulation sink and aerosol Fuchs surface area. To better characterize this, we introduce a dimensionless parameter (S)—the ratio of the max-normalized net coagulation sink to the apparent emission rate—which effectively describes particle survival at specific sizes and offers a critical and previously lacking metric to evaluate nanoparticle persistence versus suppression in indoor environments. When this ratio exceeds 10, the concentration of 1−6 nm nanoparticles is suppressed by more than a hundred-fold. However, since this ratio typically remains <10 for most 1−6 nm nanoparticles, they persist at high concentrations, posing significant health risks due to their potential to penetrate deeply into the human respiratory tract, quantified through another novel parameter—the respiratory survival probability.

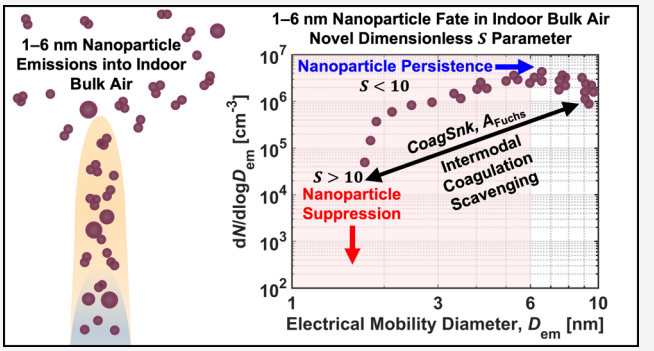

KEYWORDS: *indoor air quality, particulate matter, nanoparticle emissions, aerosol dynamics, combustion aerosol, nanoparticle coagulation*

1. INTRODUCTION

Indoor combustion has long sustained our daily routines, providing comfort, food, and utilities, while influencing the air quality around us. One significant impact on air quality arises from combustion-generated particles, which range from incipient soot particles as small as ∼1 nm to mature soot aggregates larger than 1 μm.[1] Among these are nano-organic carbon (NOC) particles:[2−4] small combustion-generated particles characterized by relatively low molar carbon-to-hydrogen (C/H) ratios (∼1.5−2.5) and sizes typically between 1 and 6 nm.[1] Studying NOC particles is essential due to their exceptionally high surface area-to-volume ratios and their surfaces, which are often coated with adsorbed volatile and semivolatile organic species.[5] However, their small size also subjects them to high diffusivities in air, making them susceptible to losses through coagulation with larger particles.[6] Remarkably, in environments with strong nanoparticle emission sources−such as new particle formation events from low-volatility oxidized gases−the source strength of nanoparticles can offset these coagulation losses,[7−9] allowing nanoparticles to persist in indoor bulk air.[10,11] While studies have characterized NOC particles down to 1 nm in flames,[12−19] the behavior and fate of the smallest NOC particles in indoor bulk air remain largely unexplored. This gap exists primarily due to the analytical challenges associated with real-time detection and sizing of atmospheric particles as small as 1 nm.[20]

Recent advancements in differential mobility analyzers (DMAs) and particle size magnification (PSM) techniques have enabled real-time detection of atmospheric nanoparticles down to 1 nm,[21] providing a timely opportunity to leverage these technologies to investigate the previously unexplored fate of the smallest atmospheric nanoparticles in the NOC size range in indoor bulk air. For centuries, candles have served not only as sources of light but also as valuable tools for advancing our fundamental understanding of combustion processes and as a source of indoor air pollution.[22,23] However, due to earlier

Received: April 27, 2025
Revised: November 8, 2025
Accepted: November 10, 2025
Published: December 25, 2025

technological constraints in atmospheric particle sizing and detection, combustion-generated candle particles have only been characterized down to ~2.3 nm,[24,25] leaving the fate of even smaller particles uncharacterized. These unexplored, sub-2.3 nm nanoparticles potentially include structurally unique forms of carbon such as fullerenes and nanodiamonds,[1,22] which are known to induce cytotoxic, apoptotic, and pro-inflammatory responses in eukaryotic and endothelial cells.[26−28] Moreover, upon inhalation, these 1−6 nm nanoparticles exhibit significant deposition in the head airways and tracheobronchial regions of the respiratory tract.[29] Their small sizes enable them to readily translocate across cellular barriers, enter the bloodstream, and potentially affect other organs, including the brain.[30−32] Recent studies have further indicated that short-term human exposure to candle combustion particles could diminish executive cognitive functioning.[33] Therefore, the possibility emerges that candle combustion-generated sub-2.3 nm nanoparticles could persist in indoor air, raising critical questions: To what concentrations do these atmospheric nanoparticles persist? Do their concentrations remain elevated down to 1 nm, or are they rapidly lost via coagulation, and what factors govern their survival in indoor bulk air? Given candles' historical and practical role in elucidating combustion phenomena,[22] we can address these fundamental questions by studying 1−6 nm atmospheric nanoparticle emissions during indoor candle combustion.

In this study, we utilized a novel nanomobility particle size spectrometer, combining a particle size magnifier with a scanning mobility particle sizer (PSMPS),[34] to investigate indoor atmospheric 1−6 nm nanoparticle dynamics during scented candle combustion within a mechanically ventilated residential test house. This allowed us to address fundamental questions regarding the fate and persistence of combustion-generated nanoparticles down to ~1 nm in indoor bulk air. The high-resolution, size-resolved, real-time measurements obtained with the PSMPS enabled the first-ever detailed exploration of coagulation scavenging effects acting on combustion-generated 1−6 nm nanoparticles. Specifically, we quantified the coagulation scavenging potential of the indoor atmosphere using the coagulation sink[35] and aerosol Fuchs surface area[36] resolved both temporally and by particle size, providing novel insights into the dynamics controlling nanoparticle survival indoors. Furthermore, we introduce a generalizable coagulation scavenging parameter that accounts for both coagulation sink strength and net apparent emission rates of 1−6 nm nanoparticles, offering a new means to predict and explain their persistence or suppression at various sizes in indoor bulk air. Importantly, our findings reveal that substantial concentrations of 1−6 nm nanoparticles survive in indoor air, significantly enhancing their potential for respiratory exposure. To address this exposure risk, we also introduce a second novel parameter, the respiratory survival probability, which quantifies the likelihood of nanoparticle deposition within different respiratory tract regions of indoor occupants. Collectively, our results not only clarify the previously unexplored persistence of nanoparticles in the NOC size range indoors but also present parameters applicable to other common household nanoparticle sources, enabling broader investigations into nanoparticle fate, exposure, and associated health risks.

2. MATERIALS AND METHODS

2.1. Field Measurements of Candle Combustion in the Purdue zEDGE Test House. Field measurements of scented candle combustion were performed in a single-zone, mechanically ventilated residential test house, called the Purdue zero Energy Design Guidance for Engineers (zEDGE) test house. Comprehensive details about the test house, including its surface materials, can be found elsewhere.[6,10,11,37−39] Briefly, the total conditioned interior volume of the test house is 60.35 m^3. The climate control within the house is managed by a ductless single-zone heating and cooling system (FTX12NMVJU, Daikin North America LLC, Houston, Texas, U.S.) and a portable air conditioning unit with an exhaust duct (QPCA08JAMWG1, Haier, Louisville, Kentucky, U.S.), which together maintained a nominal indoor air temperature of 20 °C (68 °F) throughout the study. Additionally, the test house is equipped with a variable-speed powered ventilator which included two MERV 13 filters, facilitating the influx of filtered air from outside. The operational parameters of both the powered ventilator and the portable air conditioner were adjusted to regulate the desired outdoor air ventilation rate, monitored daily using carbon dioxide (CO_2) tracer gas injection and decay. To promote air mixing in the test house, four mixing fans were installed, and the well-mixed state of particles and gases in the indoor air has been empirically validated.[6,38]

We conducted combustion activities using four different scented candles (A, B, C, and D) in the test house. Candles A, B, and C used fiber wicks, while Candle D featured a wooden wick. Combustion for each candle type was replicated three times, totaling 12 candle combustion activities. For each activity, four identical scented candles were lit simultaneously, except for Candle D, where only two were used. The combustion activities for Candle A occurred at a nominal outdoor air ventilation rate of 0.5 h^{-1}, while other candle combustion activities were conducted at 6.5 h^{-1}. Each activity began with two occupants bringing the scented candles into the house and waiting for 10 min (background period), then lighting (using a hand-held electric lighter) the candles for a twenty-minute steady burn period (source period). At the thirty-minute mark, the occupants extinguished the candles, took them, and exited the house, initiating the decay period: 2 h for Candle A (lower ventilation rate) and 1 h for the others. Afterward, the test house was purged with increased outdoor air ventilation rates for at least 20 min to reestablish background particle levels. Table S1 summarizes candle fragrances, quantities burned, and nominal outdoor air ventilation rates for all combustion activities.

2.2. Indoor Atmospheric Nanoparticle Measurements. Indoor atmospheric nanoparticle number concentrations and size distributions, ranging from 1.18 to 55.7 nm, were measured in real-time using a novel particle size magnifier−scanning mobility particle sizer (PSMPS; GRIMM Aerosol Technik Ainring GmbH & Co. KG, Ainring, Germany) for all 12 candle combustion activities. The PSMPS, a newly commercialized nanomobility particle size spectrometer, specializes in the electrical mobility-classified measurements of atmospheric nanoparticles down to 1 nm.[6,10,11,34] It integrates several components: a soft X-ray neutralizer (Model 5524-X, GRIMM Aerosol Technik Ainring GmbH & Co. KG, Ainring, Germany), a Vienna-type modified short-DMA (S-DMA; also from GRIMM Aerosol Technik

https://doi.org/10.1021/acs.est.5c05577
Environ. Sci. Technol. 2026, 60, 834−846

Ainring GmbH & Co. KG, Ainring, Germany), a diethylene glycol-based PSM (Model A10, Airmodus Ltd., Helsinki, Finland), and a butanol-based condensation particle counter (CPC; Model 5417, GRIMM Aerosol Technik Ainring GmbH & Co. KG, Ainring, Germany). The PSMPS recorded a new particle number size distribution every 120 s. Further details about the instrument's configuration, setup, and operation are available in Patra et al.[6]

In all the triplicate candle combustion activities with Candle A, in addition to the PSMPS, atmospheric particle number concentrations and size distributions from 13.1 to 572.5 nm were measured using a scanning mobility particle sizer (SMPS) with a long-DMA (Model 3938NL88, TSI Inc., Shoreview, Minnesota, U.S.).[40] Furthermore, particle number concentrations and size distributions from 500 to 10,000 nm were measured using a wideband integrated bioaerosol sensor (WIBS; Model WIBS-NEO, Droplet Measurement Technologies LLC, Longmont, Colorado, U.S.).[41] The SMPS integrated the following components: a Kr-85 bipolar charger (370 MBq, Model 3077A, TSI Inc., Shoreview, Minnesota, U.S.), a long-DMA (Model 3081, TSI Inc., Shoreview, Minnesota, U.S.), and a water-based CPC (Model 3788, TSI Inc., Shoreview, Minnesota, U.S.). It facilitated the detection of particles classified by their electrical mobility, recording a new particle number size distribution every 120 s. Concurrently, the WIBS used a 635 nm continuous laser diode for optical detection and sizing of atmospheric particles at a time resolution greater than 1 Hz,[42] which were aggregated and averaged every 120 s to align with the time resolution of both the PSMPS and SMPS. Additional details about the instruments' configuration, setup, and operational parameters are available elsewhere.[6]

For all other candle combustion activities, in addition to the PSMPS, a high-resolution electrical low-pressure impactor (HR-ELPI+; Dekati Ltd., Kangasala, Finland) was used to measure atmospheric particle number concentrations and size distributions spanning aerodynamic diameters from 6 to 10,000 nm.[43] These were recorded at 1 Hz and then averaged every 120 s. The HR-ELPI+ features a corona charger, a 14-stage low-pressure cascade impactor with electrometers, and oil-soaked sintered plates to prevent particle bounce and overload.[44] A 1.2 m conductive silicone tube was attached to the inlet of the HR-ELPI+ to sample indoor atmospheric particles. The instrument uses a sophisticated algorithm to improve particle size resolution, increasing the number of size bins from 14 to 100.[45] Further information about the instrument's configuration, setup, and operational parameters are available elsewhere.[43]

Overall, Candle A combustion activities involved measuring indoor atmospheric particles from 1.18 to 10,000 nm using the PSMPS, SMPS, and WIBS. For candles B, C, and D, measurements were made using the PSMPS and HR-ELPI+. Figure S1 shows the layout of the test house and the positioning of the instruments used during the scented candle combustion activities within the test house.

2.3. Particle Number Size Distribution Analysis. The particle number size distributions measured by the PSMPS in the sub-3 nm size fraction are affected by instrument-generated charger ions.[6,10,11] Previous studies developed a data-driven method for charger ion correction using a threshold value from background measurements.[10,11] We employed a similar charger ion correction using a 99th percentile threshold from sub-3 nm number size distributions measured during candle combustion background periods. This threshold was chosen because lower thresholds increased residual noise (Figure S2), while a 99th percentile threshold provided more reliable results without compromising the number size distributions during candle combustion periods.[6] This charger ion correction for a representative candle combustion example is presented in Figure S2. Additionally, the data acquisition software of the PSMPS corrected the measured particle number size distributions for the charging efficiency of the soft X-ray neutralizer, DMA penetration, and the combined PSM and CPC counting efficiency. An additional correction was applied for diffusional losses of nanoparticles in the soft X-ray neutralizer.

We used unmodified particle number size distributions from the SMPS from 13.1 to 200 nm. Due to SMPS limitations,[46−48] we corrected the particle number size distributions between 200 and 572.5 nm using monotonic cubic spline interpolation. The merging of particle number size distributions from the PSMPS, SMPS, and WIBS to achieve continuous particle number size distributions from 1.18 to 10,000 nm is detailed elsewhere.[6] For the HR-ELPI+, we employed the methods outlined by Wu et al.[49] to convert aerodynamic diameter-based particle number size distributions to electrical mobility diameter-based distributions. For this conversion, we used effective densities of 1.5 g cm^{-3} for sub-100 nm particles and 0.3 g cm^{-3} for larger particles, consistent with the median reported values for ultrafine and soot-mode combustion particles.[50] We used these median values rather than a size-resolved effective density to simplify the iterative calculations. To merge particle number size distributions from the PSMPS and HR-ELPI+ into continuous distributions from 1.18 to 10,000 nm, we used charger ion-corrected PSMPS data from 1.18 to 20 nm, a weighted average data of both instruments from 20 to 40 nm, and HR-ELPI+ data from 40 to 10,000 nm. Figure S3 shows the merging of a representative PSMPS and HR-ELPI+ particle number size distribution during candle combustion.

2.4. Size-Resolved 1−6 nm Nanoparticle Dynamics in Indoor Bulk Air. The charger ion-corrected particle number size distributions measured by the PSMPS within the size range of 1.18 to 6 nm were integrated to obtain size-integrated 1−6 nm particle number concentrations (N_{1-6nm}; cm^{-3}). These particles represent those emitted from the flame that persist in the bulk air after undergoing various loss processes. The aerosol general dynamics equation can be applied to these measured data and the known particle source and loss processes to estimate the apparent emission rate (E_{app}; min^{-1}) of total 1−6 nm nanoparticles released from the flame into the indoor bulk air.[6] Considering known indoor particle source and loss processes, the aerosol dynamics equation can be expressed as follows:[6,10,11]

$$E_{app,d_{p,i}}\,[\mathrm{min}^{-1}] = V\cdot\left(\frac{dN_{d_{p,i}}}{dt} + k_{vent}\cdot N_{d_{p,i}} + k_{dep,d_p}\cdot N_{d_{p,i}} + CoagSnk_{d_p}\cdot N_{d_{p,i}} - CoagSrc_{d_p}\right) \quad (1)$$

Particles in a PSMPS size bin i represent those at diameter $d_{p,i}$, which is the midpoint of that PSMPS size bin. V is the conditioned interior volume of the test house. $N_{d_{p,i}}$ is the total number of particles in the size bin represented by the diameter

https://doi.org/10.1021/acs.est.5c05577
Environ. Sci. Technol. 2026, 60, 834−846

$d_{p,i}$. The first term on the RHS of eq 1 represents the temporal rate of range of $N_{d_{p,i}}$. The second and third terms on the RHS of eq 1 represent the loss of particles due to ventilation and deposition onto indoor surfaces via Brownian and turbulent diffusion, respectively. k_{vent} [min^{-1}] is the outdoor air ventilation rate, nominally 0.5 or 6.5 h^{-1}, and k_{dep,d_p} [min^{-1}] is the size-dependent first-order deposition loss rate coefficient for particles at size d_p. k_{dep,d_p} was estimated using the Lai and Nazaroff[51] indoor particle deposition model (considering various indoor surfaces) and is detailed elsewhere.[6] The estimation of apparent emission rates for candle combustion activities in eq 1 does not include any condensational terms because we could not fit apparent condensational growth rate curves to the temporal particle number size distributions during candle combustion, due to the absence of a clear mode (Section 3.1);[52] therefore, it has been ignored in the model.

The fourth and fifth terms on the RHS of eq 1 represent size-resolved particle transformations due to coagulation dynamics. Here, the fourth term accounts for the loss of particles due to coagulation onto existing particles, while the fifth term represents the formation of particles at size d_p resulting from coagulation. The term $CoagSnk_{d_p}$ [min^{-1} or h^{-1}] describes the particle loss rate at size d_p due to coagulation with the pre-existing particle population, and is expressed as follows:[53]

$$CoagSnk_{d_p} = \sum_{d'_p=1.18nm}^{d'_p=10,000nm} k_{coag}(d_p, d'_p)\cdot N_{d'_{p,i}} \quad (2)$$

k_{coag} is the coagulation coefficient between two particles and is calculated using the Brownian and van der Waals viscous forces coagulation model.[6] The Hamaker constant used in the model for candle combustion activities is 3.5×10^{-19} J, corresponding to the Hamaker constant reported for flame-formed carbon nanoparticles.[54] The term $CoagSrc_{d_p}$ [cm^{-3} min^{-1}] parametrizes the formation of particles at size d_p due to coagulation, and is expressed as follows:[6]

$$CoagSrc_{d_p} = \sum_{d_p^3=d'^3_p+d''^3_p}^{d'_p,d''_p<d_p} 0.5\cdot k_{coag}(d'_p, d''_p)\cdot N_{d'_{p,i}}\cdot N_{d''_{p,j}} \quad (3)$$

Thus, coagulation in the bulk air can result in both the loss of particles and the formation of new particles at a given size d_p. The net effect of coagulation is parametrized using the net coagulation sink[53] ($CoagSnk_{Net}$; h^{-1}), and is expressed as follows:

$$CoagSnk_{Net,d_p} = CoagSnk_{d_p} - \frac{CoagSrc_{d_p}}{N_{d_{p,i}}} \quad (4)$$

Coagulation dynamics play a dominant role in particle transformation in both indoor and outdoor environments during periods of active emissions.[6,10,55] However, limited information is available on the net coagulation sink values during indoor combustion, which are expected to significantly influence the fate of combustion-generated particles, particularly in the NOC size range, due to their smaller sizes. Estimating coagulation sinks is computationally complex (as illustrated by eqs 2–4). A representative parameter, the aerosol Fuchs surface area[36] (A_{Fuchs}; μm^2 cm^{-3}), derived from kinetic theory, serves as an effective proxy of coagulation potential and has been shown to accurately capture coagulation scavenging effects.[36] A_{Fuchs} is calculated as follows:

$$A_{\mathrm{Fuchs}} = \frac{4\pi}{3}\int_{d_p=1.18nm}^{d_p=1,000nm} d_p^2\cdot\left(\frac{Kn + Kn^2}{1 + 1.71Kn + 1.33Kn^2}\right)\cdot \frac{dN}{d\log D_p}\cdot d\log D_p \quad (5)$$

The computation of A_{Fuchs} is straightforward and requires only the particle number size distribution and the particle Knudsen number (Kn), defined as the ratio of the mean free path of air to the particle radius. A_{Fuchs} can also be expressed as a function of size by differentiating both sides of eq 5 with respect to $\log D_p$ yielding:

$$\frac{dA_{Fuchs}}{d\log D_p} = \frac{4\pi}{3}\cdot d_p^2\cdot\left(\frac{Kn + Kn^2}{1 + 1.71Kn + 1.33Kn^2}\right)\cdot\frac{dN}{d\log D_p} \quad (6)$$

Both A_{Fuchs} and $CoagSnk_{Net,d_p}$ characterize the coagulation scavenging potential of the immediate environment.[36,53] While these parameters are well-documented for outdoor environments,[52,53,55−57] corresponding data for indoor environments remain scarce. Due to this lack of established indoor A_{Fuchs} and $CoagSnk_{Net,d_p}$ values, clear criteria for determining the suppression or survival of nanoparticles indoors do not currently exist. For outdoor environments, similar parameters—such as the McMurry L parameter and its variations[58,59]—are already in use to determine whether a new particle formation event will occur. Inspired by the theoretical framework of the McMurry L parameter, we introduce a dimensionless parameter, S, specifically designed to assess the suppression or survival of nanoparticles at various sizes in indoor environments. The parameter S is defined as the ratio between the maximum normalized $CoagSnk_{Net,d_p}$ and the maximum normalized $E_{app,d_{p,i}}$, within a given particle size interval, expressed as follows:

$$S = \frac{\left(\frac{CoagSnk_{Net,d_p}}{\max(CoagSnk_{Net,d_p})\rfloor_{d_{p,1}\to d_{p,2}}}\right)}{\left(\frac{E_{app,d_{p,i}}}{\max(E_{app,d_{p,i}})\rfloor_{d_{p,1}\to d_{p,2}}}\right)} \quad (7)$$

This new dimensionless criterion, S, represents the ratio between the normalized dominant loss rate and the normalized apparent emission rate of particles. It can, therefore, predict whether particles of a particular size will persist or be suppressed in indoor bulk air. Higher values of S indicate that losses dominate emissions, resulting in particle suppression, while lower values imply particle persistence.

Finally, since occupants are frequently present in indoor environments, it is essential to assess the respiratory risks posed by particles that persist in the indoor bulk air. Traditionally, respiratory risk is evaluated by calculating the respiratory tract deposited dose rates (R_D; min^{-1}) across various respiratory tract regions, namely the head airways (HA), tracheobronchial (TB), and pulmonary (P) regions.[43,60] These dose rates can be determined using established methods described elsewhere.[6,43] Here, we introduce an additional parameter: the respiratory survival probability of particles within each respiratory tract region, expressed as follows:

https://doi.org/10.1021/acs.est.5c05577
Environ. Sci. Technol. 2026, 60, 834−846

$$\text{Respiratory Survival Probability} = \frac{\overline{R_{D,i(HA/TB/P)}}_{Source}}{\overline{E_{app,d_{p,i}}}_{Source}} \quad (8)$$

$\overline{R_{D,i(HA/TB/P)}}_{Source}$ is the mean size-resolved respiratory tract deposited dose rate during the source period, and $\overline{E_{app,d_{p,i}}}_{Source}$ is the mean size-resolved apparent emission rate during the same period. This parameter normalizes respiratory tract deposited dose rates by the corresponding apparent emission rates, creating a generalizable respiratory exposure metric that facilitates comparison across different particle sources.

3. RESULTS AND DISCUSSION

3.1. Indoor Atmospheric Nanoparticles Measured Down to 1.18 nm During Scented Candle Combustion.

A series of complex physical and chemical transformations convert melted wax into soot particles within a candle flame (Figure 1).[1,61] At the flame's center near the wick, melted wax drawn upward by capillary action undergoes thermal decomposition, forming gas-phase hydrocarbons and soot precursor species.[61] These precursor species transition into condensed-phase particles through a continuous mechanism known as particle inception.[62] Following soot inception, the newly formed incipient soot particles experience rapid surface growth and coagulation, evolving into larger primary particles and eventually into mature soot particles.[1] However, nanoparticles in flames exhibit low coagulation rates at high temperatures due to weak van der Waals interactions relative to their thermal energy,[63] preventing some incipient soot particles from coagulating. Additionally, fragmentation of mature soot particles into smaller ones[64,65] further diversifies particle sizes within the flame. Consequently, particle number size distributions measured near the flame tip encompass a broad size range: from incipient soot particles (~1 nm) to mature soot particles (>100 nm).[12,13,17,19,63,66,67]

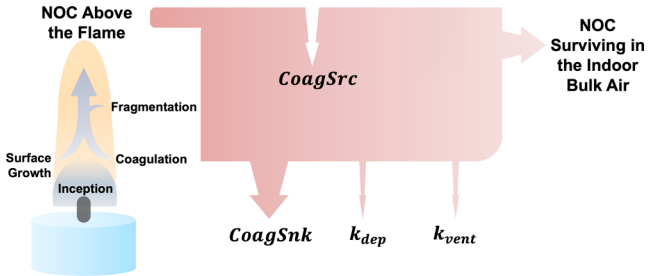

Figure 1. Schematic illustration of the journey of NOC particles from their inception in the flame to their persistence in indoor bulk air, despite undergoing various physical and chemical transformations. These NOC particles likely constitute the 1−6 nm atmospheric nanoparticles measured by the PSMPS in the indoor bulk air.

NOC particles constitute a subset of this broad size range of combustion-generated particles, ranging from 1 to 6 nm in size, including incipient soot particles and growth centers.[1] Studies have identified flame-generated fullerenes and nanodiamonds within this NOC size range directly inside candle flames.[22] However, once emitted outside the flame, additional particle loss mechanisms become significant (Figure 1). Such losses include removal through ventilation and deposition onto indoor surfaces. Furthermore, the particle emissions from flames span both smaller NOC particles and larger soot particles.[1] The larger indoor air volume provides extended residence times, increasing the likelihood of coagulation between these particles, thereby enhancing the loss of NOC particles through coagulation in real-world indoor atmospheres. Thus, for NOC particles to persist in indoor environments, they must overcome these loss mechanisms in the bulk indoor air after being formed and emitted from the flame (Figure 1).

Interestingly, our findings provide strong evidence that despite various particle loss mechanisms, continuous and significant emissions of nanoparticles in the NOC size range from candle flames lead to persistently high concentrations of these particles in the indoor bulk air (Figure 2, top and fourth rows). We measured sustained high concentrations of size-integrated 1−6 nm nanoparticles ($N_{1-6\ nm}$) in indoor bulk air before their eventual growth into mature soot particles, with median $N_{1-6\ nm}$ values of 7.4×10^5 cm^{-3} (IQR: 2.7×10^5−1.2×10^6 cm^{-3}) during scented candle combustion.

Prior studies report the formation of 1−6 nm liquid-like, condensed-phase NOC particles in flames.[1] Therefore, the 1−6 nm nanoparticles we measured in bulk indoor air may include carbonaceous species such as incipient soot, fullerene-like and nanodiamond-like clusters, and fragmented soot.[1,19,22,67] Additionally, a recent study provides experimental evidence that pyrolysis soot particles larger than 1.5 nm are in the particulate phase and exhibit low volatility, showing little evaporation even above 900 K.[68] Evidence now suggests that 1−6 nm particles persist in indoor air at concentrations of millions per cm^3 of indoor air. Although a minimal fraction of these nanoparticles may originate from the lighter used to ignite the candles, the lighter's impact is negligible because it was only employed at the start (10 min mark) of the source period, whereas elevated 1−6 nm nanoparticle concentrations persisted throughout the full twenty-minute combustion period. It is also possible that some 1−6 nm nanoparticles are secondary nanoparticles formed due to the ozonolysis of emitted monoterpenes from scented candles; however, recent research indicates that monoterpene ozonolysis is substantially suppressed in the presence of candle combustion, resulting in minimal formation of secondary organic aerosol.[69] This suppression is primarily attributed to the reduced formation of extremely low-volatility organic compounds due to elevated nitrogen monoxide concentrations (>2 ppb) emitted during combustion.[70] Additionally, ozone availability is further limited by reactions with emitted nitrogen oxides, reducing its role in oxidation processes.[71] Therefore, the observed 1−6 nm nanoparticles likely originate predominantly from the candle combustion process itself. Given our direct observations of persistently high indoor concentrations of 1−6 nm nanoparticles, future research is necessary to confirm their detailed chemical composition in indoor bulk air.

The high-resolution size-resolved data obtained from the PSMPS allowed, for the first time, an in-depth characterization of the particle number size distributions of 1−6 nm nanoparticles in indoor bulk air (Figures 3 (top-left) and S4). This enabled the identification of a significant sub-10 nm particle mode that falls distinctly within the NOC particle size range (Figure S4), highlighting their substantial contribution to the overall particle population emitted by candle flames. Quantitatively, 1−6 nm nanoparticles constitute up to ~65% of the total particle population persisting indoors during candle combustion (Figure 3 (top-right)). Notably, however, nanoparticles smaller than 1.5 nm were observed not to persist in

https://doi.org/10.1021/acs.est.5c05577
Environ. Sci. Technol. 2026, 60, 834−846

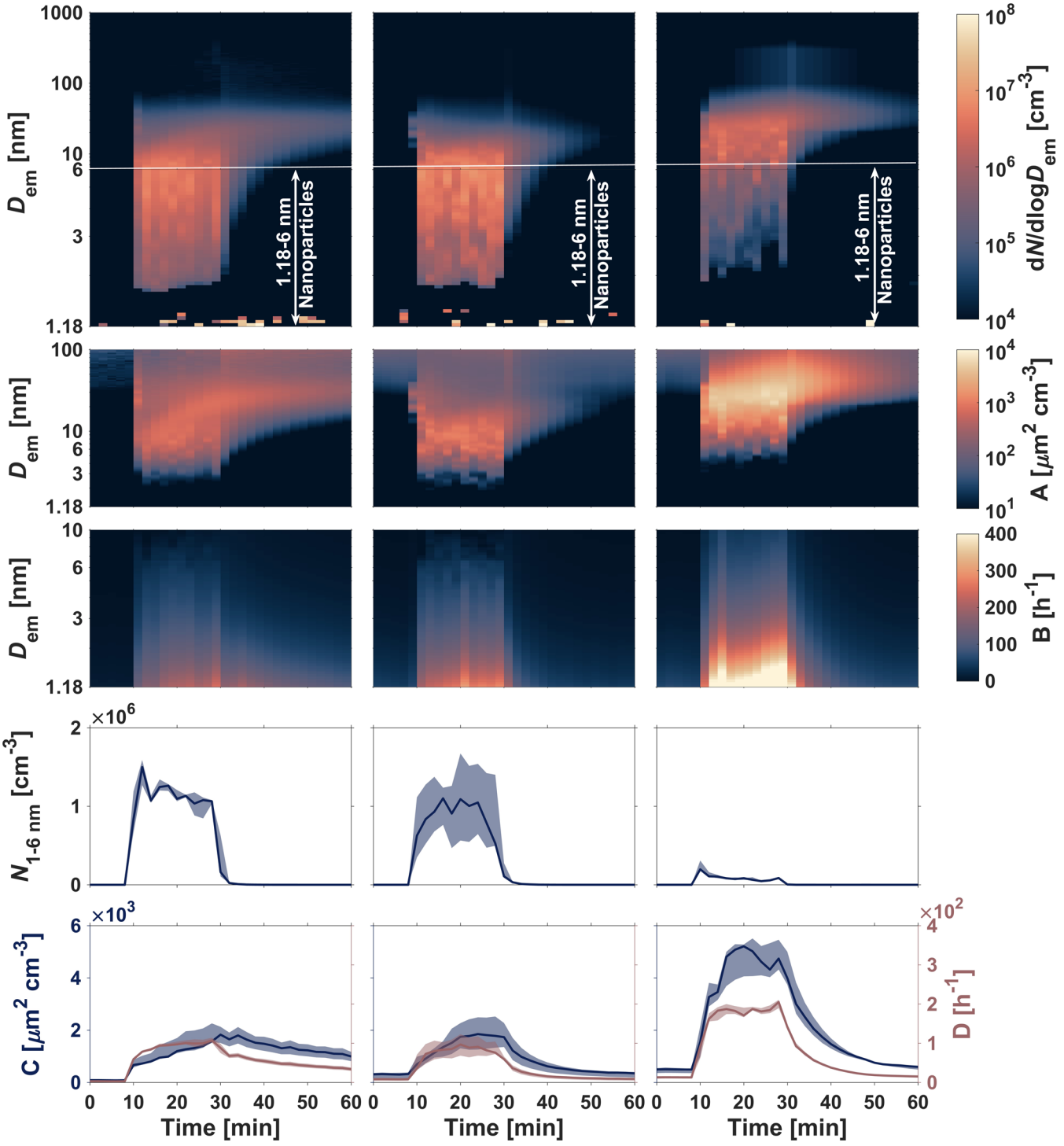

Figure 2. Time-resolved evaluation of (top row) indoor atmospheric particle number size distributions, (second row) aerosol Fuchs surface area size distributions, (third row) size-resolved net coagulation sink, (fourth row) size-integrated 1.18−6 nm nanoparticle number concentrations, and (bottom row, left *y*-axis) aerosol Fuchs surface area with (bottom row, right *y*-axis) net 1−6 nm nanoparticle coagulation sink during indoor scented candle combustion in the Purdue zEDGE test house. Left column: scented candle combustion at an outdoor air ventilation rate of 0.5 h^{-1} (Candle A); middle column: scented candle combustion at an outdoor air ventilation rate of 6.5 h^{-1} (Candle B and C); right column: wooden wick candle combustion at an outdoor air ventilation rate of 6.5 h^{-1} (Candle D). The top three rows present size-resolved distributions of representative examples for each column (particle number size distributions for all candle combustion activities are presented in Figure S5). The bottom two rows display the median values using solid lines and the 25th−75th percentile values within the shaded areas. The *y*-labels with alphabets indicate: A: $dA_{Fuchs}/d\log D_{em}$; B: $CoagSnk_{Net}$; C: A_{Fuchs}; D: $CoagSnk_{Net,1-6\ nm}$. The arrow on the top plot represents the 1.18−6 nm nanoparticle size range.

the bulk air (Figure 3 (top-left)). Previous studies have only characterized candle combustion particles down to 2.3 nm in the indoor bulk air, leaving the fate of sub-2.3 nm particles largely unknown.

https://doi.org/10.1021/acs.est.5c05577
Environ. Sci. Technol. 2026, 60, 834−846

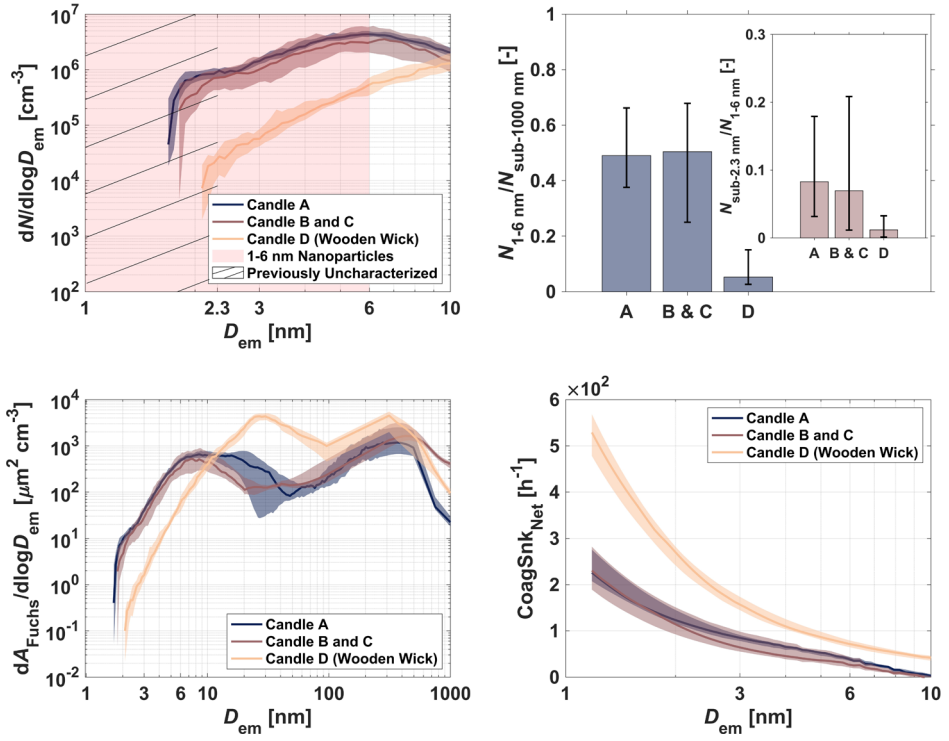

Figure 3. (top left) Median sub-10 nm particle number size distributions during the source emission period of indoor scented candle combustion activities; (top right) median ratio of size-integrated 1.18−6 nm nanoparticle number concentrations to size-integrated sub-1000 nm number concentrations during the source emission period of indoor scented candle combustion activities with inset plot representing the median ratio of size-integrated sub-2.3 nm number concentrations to size-integrated 1.18−6 nm nanoparticle number concentrations during the same period; (bottom left) median aerosol Fuchs surface area size distributions during the source emission period of indoor scented candle combustion activities; (bottom right) median size-resolved net coagulation sink during the source emission period of indoor scented candle combustion activities. The shaded areas represent the 25th−75th percentile values and the error bars represent the minimum and maximum values.

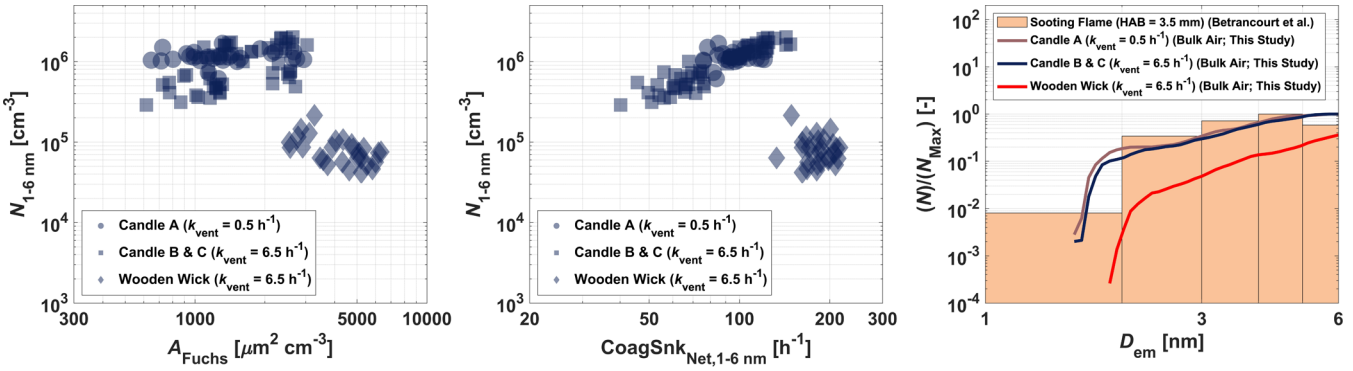

Figure 4. (left) Relationship between the aerosol Fuchs surface area and the size-integrated 1.18−6 nm nanoparticle number concentrations; (middle) relationship between the net 1.18−6 nm nanoparticle coagulation sink and the size-integrated 1.18−6 nm nanoparticle number concentrations; (right) size-resolved, normalized 1.18−6 nm nanoparticle number concentrations during the source emission period of indoor scented candle combustion activities (this study) compared against 1−6 nm nanoparticle number concentrations, measured down to 1 nm at a height of 3.5 mm above the burner of a sooty flame, as reported by Betrancourt et al.[19]

Here, we provide direct evidence that nanoparticles in the NOC size range during candle combustion do indeed persist, down to below 2.3 nm in the indoor bulk air, contributing up to ∼20% of the total 1−6 nm nanoparticle concentrations (Figure 3 (top-right)), yet surprisingly disappear below 1.5 nm. This observation highlights a unique and previously undocumented interplay between particle suppression and persistence during candle combustion. While earlier literature on sooting flames indicates persistence of incipient soot particles down to ∼1 nm at close proximities above burners (3.5 mm height, Figure 4 (right)),[19] our findings explicitly demonstrate that sub-1.5 nm nanoparticles fail to persist in indoor bulk air (Figures 3 (top-left) and 4 (right)). This suggests that while the sub-1.5 nm particles escape the flame, they fail to persist in the indoor bulk air. Overall, despite the high concentration of 1−6 nm nanoparticles indoors, a suppression occurs at sizes below 2 nm (Figure 3 (top-left)), with complete disappearance at sizes below 1.5 nm. The underlying processes controlling this intriguing interplay between particle suppression and persistence are explored in detail in the subsequent subsections.

https://doi.org/10.1021/acs.est.5c05577
Environ. Sci. Technol. 2026, 60, 834−846

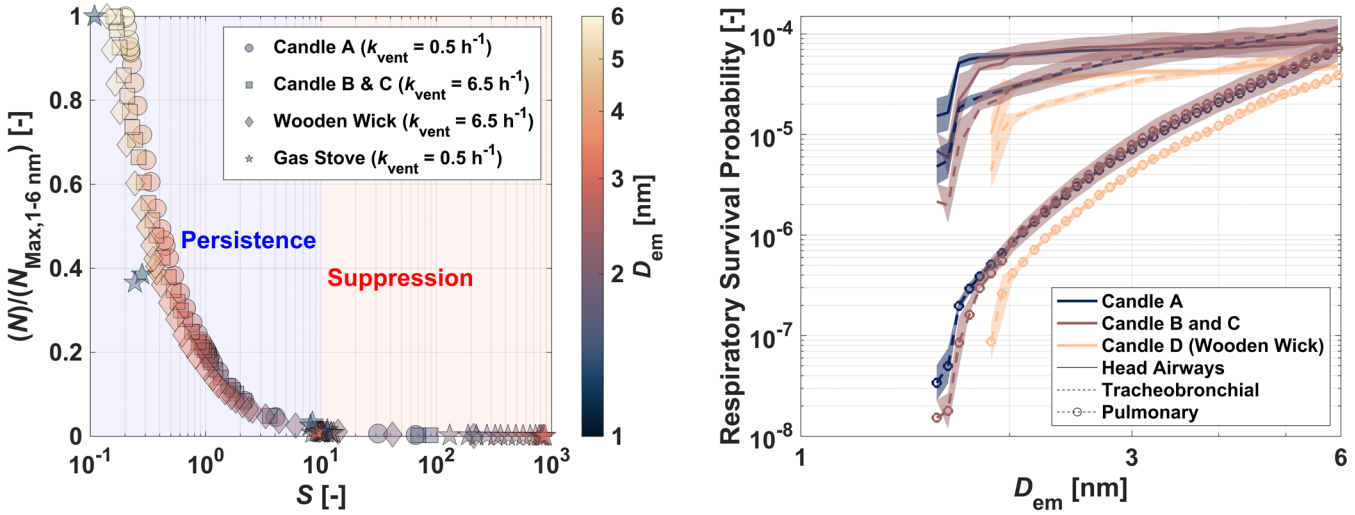

Figure 5. (left) Relationship between normalized 1.18−6 nm nanoparticle number concentrations (across 1−6 nm size fractions) and the dimensionless parameter S (calculated using eq 7) during the source emission period of indoor scented candle combustion activities. $S > 10$ indicates nanoparticle suppression, while $S < 10$ indicates nanoparticle persistence in the indoor bulk air. Data points for the gas stove are taken from Patra et al.[6] (right) Size-resolved respiratory survival probability (calculated using eq 8) across different regions of the respiratory tract (head airways, tracheobronchial, and pulmonary) during the source emission period of indoor scented candle combustion activities. Colored lines represent different candle types, while line styles represent different respiratory tract regions.

3.2. Evaluation of the Coagulation Scavenging Potential of the Indoor Atmosphere Using the Indoor Aerosol Fuchs Surface Area and Coagulation Sink. The emission characteristics of combustion-generated particles varied among different candle types, notably with Candle D, featuring a wooden wick, emitting higher quantities of larger particles compared to Candles A, B, and C (Figures 2 (top row), 3 (top-left), and S4)). This is likely because the wooden wick in candle D burns less uniformly and intermittently smolders, yielding a greater number of larger particles. The presence of a greater number of larger atmospheric particles increases the total available particle surface area,[72] thereby enhancing the coagulation scavenging potential of the indoor atmosphere. This enhanced scavenging potential occurs because larger particle surface areas efficiently facilitate interactions, especially with smaller particles, leading to effective coagulation and subsequent removal.[6] To quantitatively evaluate this process, parameters such as the net coagulation sink ($CoagSnk_{Net}$), representing the modeled coagulation sink of particles, and the aerosol Fuchs surface area (A_{Fuchs}), a kinetic theory-based proxy for coagulation scavenging, are employed, as detailed in Section 2.4.

Candle combustion significantly increased the indoor air coagulation scavenging potential by an order of magnitude (Figure 2, bottom row). Here, we provide the first-ever size-resolved and time-resolved data on coagulation scavenging potential within indoor atmospheres estimated for sub-2.3 nm nanoparticles (Figure 2: second, third, and bottom rows; and Figure 3: bottom-left and bottom-right). The indoor air coagulation scavenging potential remained elevated throughout active candle combustion, primarily due to the presence of a secondary particle mode observed at sizes greater than 100 nm during candle combustion activities (Figure S4). This mode became dominant in the size-resolved A_{Fuchs} distributions (Figure 3 (bottom-left)). The net coagulation sink values ($CoagSnk_{Net}$) increased monotonically with decreasing particle diameter (Figure 3 (bottom-right)), indicating very high coagulation loss rates for smaller particles, particularly those below 2 nm, where $CoagSnk_{Net}$ exceeded 100 h^{-1}. For context, typical outdoor air ventilation rates in residential urban homes range from ∼0.4 to 1.6 h^{-1},[73] and indoor deposition rates from common surfaces typically reach up to 5 h^{-1}.[74]

Therefore, coagulation losses during active emission periods dominate the fate of nanoparticles indoors. This explains the negligible differences observed in 1−6 nm nanoparticle persistence in indoor air despite significantly different outdoor air ventilation rates (0.5 h^{-1} vs 6.5 h^{-1}; Figure 2) during the fiber-wick candle combustion periods (Candles A, B, and C). The similarity in 1−6 nm nanoparticle persistence arises because the coagulation scavenging potentials were comparable and substantially exceeded the ventilation rates (Figure 2: second, third, and bottom rows; Figure 3: bottom-left and bottom-right). Candle D, on the other hand, which featured a wooden wick, emitted a greater number of larger particles (Figure S4). This led to a significantly higher indoor coagulation scavenging potential, resulting in noticeably fewer 1−6 nm nanoparticles persisting in the indoor bulk air during Candle D combustion (Figures 2 and 4). Thus, comprehending coagulation scavenging potential is essential for fully understanding nanoparticle dynamics in indoor environments. However, data on $CoagSnk_{Net}$ and A_{Fuchs} for indoor atmospheres remain limited; therefore, systematically quantifying these parameters for various indoor particle sources is critical to advancing our understanding of indoor atmospheric nanoparticle behavior.

The median A_{Fuchs} values for Candles A, B, and C were 1.3 × 10^3 μm^2 cm^{-3} (IQR: 1.1 × 10^3−2.2 × 10^3 μm^2 cm^{-3}), whereas Candle D had significantly higher A_{Fuchs} values (median: 4.4 × 10^3 μm^2 cm^{-3} with IQR: 3.4 × 10^3−5.2 × 10^3 μm^2 cm^{-3}). For reference, the median A_{Fuchs} values of the test house during the background period were 250 μm^2 cm^{-3} (IQR: 110−410 μm^2 cm^{-3}). Similar trends were observed for the coagulation sink of 1−6 nm nanoparticles ($CoagSnk_{Net,1-6\ nm}$)−defined as the median $CoagSnk_{Net}$ across the 1−6 nm size fraction (median $CoagSnk_{Net,1-6\ nm}$ for Candles A, B, and C were 93 h^{-1} (IQR: 69−107 h^{-1}); median $CoagSnk_{Net,1-6\ nm}$ for Candle D were 183

https://doi.org/10.1021/acs.est.5c05577
Environ. Sci. Technol. 2026, 60, 834−846

h^{-1} (IQR: 168−200 h^{-1}); and median background $CoagSnk_{Net,1-6\ nm}$ of the test house were 7 h^{-1} (IQR: 3−12 h^{-1})). Both A_{Fuchs} and $CoagSnk_{Net,1-6\ nm}$ exhibited significant positive correlation with each other (Figure S6). These coagulation scavenging potentials observed indoors are comparable to, or even exceed, those reported for polluted urban outdoor areas (A_{Fuchs}: 10^2−10^3 μm^2 cm^{-3}; $CoagSnk_{Net}$∼70 h^{-1}).[36,57] This suggests that indoor air coagulation scavenging potentials can match or surpass outdoor levels, primarily due to reduced air dilution and the constrained indoor volume. Furthermore, as discussed previously, these indoor coagulation scavenging rates dominate over other particle loss mechanisms during active emission periods, thereby playing a critical role in controlling whether nanoparticles persist or are suppressed in the indoor air (discussed in the following subsection).

3.3. Fate of Indoor 1−6 nm Nanoparticles in Indoor Air: Persistence vs Suppression. 1−6 nm nanoparticles in indoor bulk air during candle combustion exhibited simultaneous persistence and suppression, characterized by the suppression of sub-2 nm particles and significant persistence of 2−6 nm nanoparticles. Notably, overall, 1−6 nm nanoparticle concentrations were lower for Candle D compared to Candles A, B, and C (Figure 4: left and middle columns), corresponding to higher coagulation scavenging potential of the indoor air during Candle D combustion. As previously established, coagulation losses dominate particle removal mechanism indoors; however, loss rates alone do not fully capture the particle dynamics, since particle persistence in indoor air reflects a balance between emission and loss processes. Thus, we introduce a dimensionless parameter, *S*, defined as the ratio of the maximum normalized net coagulation sink to the maximum normalized net apparent emission rate within the 1−6 nm size fraction, as detailed in Section 2.4. Higher values of *S* indicate loss-dominated conditions leading to particle suppression, whereas lower values imply conditions favoring particle persistence.

A clear distinction between particle persistence and suppression can be effectively demonstrated using the dimensionless *S* parameter. We observed that when *S* values exceeded 10, there was significant suppression of 1−6 nm nanoparticles at corresponding particle sizes, with concentrations falling below 1% of the maximum measured size-resolved 1−6 nm nanoparticle concentration (Figure 5 (left)). Conversely, the maximum concentrations, indicating the highest persistence, occurred at particle sizes associated with the lowest *S* values (Figure 5 (left)). Moreover, when *S* values surpassed 100, the presence of 1−6 nm nanoparticles from candle combustion became negligible. *S* exceeded 100 for particles smaller than 1.57 nm from Candles A, B, and C, and for particles smaller than 1.88 nm from Candle D, which explains their disappearance in indoor air during candle combustion.

To test the broader applicability of this parameter, we evaluated data from another study involving 1−6 nm nanoparticles emitted from a more efficient indoor combustion source, a propane gas stove.[6] The fate of 1−6 nm nanoparticles in bulk air from this different combustion source could also be explained using the *S* criterion (Figure 5 (left)). An interesting distinction between candles and gas stoves as indoor combustion sources was that candle flames exhibited lower *S* values for larger 1−6 nm nanoparticles, whereas gas stove flames showed lower *S* values for smaller 1−6 nm nanoparticles. This indicates a predominance of larger 1−6 nm nanoparticles in indoor air from candle flames, whereas smaller 1−6 nm nanoparticles dominate the indoor air from gas stove flames. Thus, our novel dimensionless *S* parameter provides a critical and previously lacking metric for evaluating nanoparticle persistence versus suppression in indoor environments, significantly enhancing our ability to assess indoor nanoparticle fate.

S values were found to be less than 10 for most 1−6 nm nanoparticles emitted by candle flames, particularly in the 2−6 nm size range (Figure 5 (left)). This low *S* value indicates that these 1−6 nm nanoparticles persist in the indoor air at high concentrations for extended periods. As a result, their potential respiratory exposure risks are elevated due to increased persistence. To quantify these risks, we introduced another novel, generalizable parameter: respiratory survival probability (as discussed in Section 2.4). This metric captures the likelihood of particles reaching and persisting in different regions of the respiratory tract. Our size-resolved analysis revealed a general increase in respiratory survival probability with particle diameter across the 1−6 nm size-fraction (Figure 5 (right)). Notably, 1−6 nm nanoparticles around 6 nm exhibited high respiratory survival probabilities (∼10^{-4}), with pulmonary survival probabilities comparable to those in the upper respiratory tract regions. This suggests that 1−6 nm nanoparticles can efficiently penetrate into even the deepest parts of the lungs, which is concerning given that scented candle combustion often occurs in occupied spaces. To contextualize the magnitude of exposure, during our combustion activities, the apparent emission rate for 6 nm particles was ∼10^{12} particles min^{-1} (Figure S7). Based on the estimated respiratory survival probabilities, ∼2 × 10^9 6 nm particles are estimated to reach each of the three respiratory regions over a 20 min exposure period. This is an alarming number, especially considering the well-documented cytotoxic and pro-inflammatory effects of combustion-generated 1−6 nm nanoparticles.[26−28] However, note that our measurements did not characterize the chemical composition of 1−6 nm nanoparticles in the bulk air from candle combustion; therefore, we cannot fully elucidate the health effects of their deposition in the human respiratory tract. As discussed in the next paragraph, further research is needed to determine the health relevance of these nanoparticles, which are deposited in the respiratory tract regions at such high doses.

3.4. Limitations and Future Outlook. Our study provides the first direct characterization of the fate and exposure of indoor atmospheric nanoparticles down to 1.18 nm during candle combustion, revealing a striking interplay between the simultaneous suppression and persistence of 1−6 nm nanoparticles in indoor bulk air. Measurements in the 1−3 nm size range can include very small particles, large gas-phase molecules, and transient molecular clusters, which cannot be distinguished with PSMPS.[52,75−78] Because we did not measure chemical composition of indoor atmospheric nanoparticles, the physical identity of the 1−3 nm PSMPS signal remains uncertain. Existing literature suggests that 1−6 nm liquid-like, condensed-phase particles form in flames[1] and are therefore likely to be among the 1−6 nm nanoparticles measured in bulk indoor air in this study. However, future studies are warranted to resolve the composition and phase of sub-10 nm indoor atmospheric nanoparticles during candle combustion. Emerging techniques that combine nanoparticle size classification with a DMA, followed by electrostatic collection onto a filament, thermal desorption of the collected

https://doi.org/10.1021/acs.est.5c05577
Environ. Sci. Technol. 2026, 60, 834−846

nanoparticles, and subsequent analysis via high-resolution chemical ionization mass spectrometry,[79] or tandem DMA-based volatility measurements,[80] would provide more information on their chemical composition, especially given our findings that sub-10 nm, particularly sub-6 nm, nanoparticles persist at high concentrations in indoor air.

Although there are limitations in the instrumentation and the general aerosol dynamics model used here,[6,10] they do not detract from the significance of the observed results. First, PSMPS measurements of 1−6 nm nanoparticles are subject to limitations related to presence of unstable clusters and subtracting the sub-3 nm charger-ion background signals, as discussed in detail elsewhere.[6,10] Second, although the literature indicates that pyrolytic soot particles larger than 1.5 nm are largely nonvolatile (Section 3.1), we lack direct volatility measurements for the 1−6 nm nanoparticles in this study. Third, the Fuchs-corrected coagulation sinks estimates assume all 1−6 nm species are particulate, which may not be valid due to the presence of unstable molecular clusters, which do not add to the particle surface area. Overall, for these reasons, modeling calculations and assessments of the health relevance for sub-3 nm nanoparticles remain uncertain; however, we applied appropriate literature-based corrections throughout, and the results should be regarded as estimates conditioned on these assumptions. Nevertheless, the introduction of novel parameters provides a critical advancement in quantifying nanoparticle persistence versus suppression, bridging a gap in indoor aerosol dynamics studies. Looking ahead, by using the parameters discussed in this study, future research can more accurately assess the coagulation scavenging potential of indoor environments and predict the fate of nanoparticles from diverse sources in indoor settings.

■ ASSOCIATED CONTENT

Supporting Information

The Supporting Information is available free of charge at https://pubs.acs.org/doi/10.1021/acs.est.5c05577.

> Summary table of candle combustion activities including details regarding candle fragrances, the number of candles burned, and nominal outdoor air ventilation rates along with median $N_{1-6\ nm}$, $CoagSnk_{Net}$, and A_{Fuchs} values during the source emission periods of these activities, and particle number size distributions for all 12 candle combustion activities (PDF)

■ AUTHOR INFORMATION

Corresponding Author

Brandon E. Boor − *Lyles School of Civil and Construction Engineering, Purdue University, West Lafayette, Indiana 47907, United States;* orcid.org/0000-0003-1011-4100; Email: bboor@purdue.edu

Authors

Satya S. Patra − *Lyles School of Civil and Construction Engineering, Purdue University, West Lafayette, Indiana 47907, United States;* orcid.org/0000-0003-2099-7875

Gerhard Steiner − *GRIMM Aerosol Technik Ainring GmbH & Co. KG, Ainring 83404, Germany*

Complete contact information is available at: https://pubs.acs.org/10.1021/acs.est.5c05577

Notes

The authors declare the following competing financial interest(s): G.S. is a full-time employee of GRIMM Aerosol Technik Ainring GmbH & Co. KG, which has a potential direct or indirect financial interest in the subject matter discussed in the manuscript.

■ ACKNOWLEDGMENTS

Financial support was provided by the National Science Foundation (CBET-1847493 to B.E.B.) and an American Society of Heating, Refrigerating, and Air Conditioning Engineers Graduate Student Grant-In-Aid Award (to S.S.P.).

■ REFERENCES

(1) Michelsen, H. A.; Colket, M. B.; Bengtsson, P.-E.; D'Anna, A.; Desgroux, P.; Haynes, B. S.; Miller, J. H.; Nathan, G. J.; Pitsch, H.; Wang, H. A Review of Terminology Used to Describe Soot Formation and Evolution under Combustion and Pyrolytic Conditions. *ACS Nano* **2020**, *14* (10), 12470−12490.

(2) D'Anna, A.; Rolando, A.; Allouis, C.; Minutolo, P.; D'Alessio, A. Nano-Organic Carbon and Soot Particle Measurements in a Laminar Ethylene Diffusion Flame. *Proceedings of the Combustion Institute* **2005**, *30* (1), 1449−1456.

(3) Paul, B.; Datta, A.; Datta, A.; Saha, A. Optical Characterization of Nano-Sized Organic Carbon Particles Emitted from a Small Gasoline Engine. *Particuology* **2013**, *11* (3), 249−255.

(4) D'Anna, A.; Commodo, M.; Violi, S.; Allouis, C.; Kent, J. Nano Organic Carbon and Soot in Turbulent Non-Premixed Ethylene Flames. *Proceedings of the Combustion Institute* **2007**, *31* (1), 621−629.

(5) Pedata, P.; Stoeger, T.; Zimmermann, R.; Peters, A.; Oberdörster, G.; D'Anna, A. "Are We Forgetting the Smallest, Sub 10 nm Combustion Generated Particles?". *Part. Fibre Toxicol.* **2015**, *12* (1), 34.

(6) Patra, S. S.; Jiang, J.; Ding, X.; Huang, C.; Reidy, E. K.; Kumar, V.; Price, P.; Keech, C.; Steiner, G.; Stevens, P.; Jung, N.; Boor, B. E. Dynamics of Nanocluster Aerosol in the Indoor Atmosphere during Gas Cooking. *PNAS Nexus* **2024**, *3* (2), No. pgae044.

(7) Wang, M.; Kong, W.; Marten, R.; He, X.-C.; Chen, D.; Pfeifer, J.; Heitto, A.; Kontkanen, J.; Dada, L.; Kürten, A.; Yli-Juuti, T.; Manninen, H. E.; Amanatidis, S.; Amorim, A.; Baalbaki, R.; Baccarini, A.; Bell, D. M.; Bertozzi, B.; Bräkling, S.; Brilke, S.; Murillo, L. C.; Chiu, R.; Chu, B.; De Menezes, L.-P.; Duplissy, J.; Finkenzeller, H.; Carracedo, L. G.; Granzin, M.; Guida, R.; Hansel, A.; Hofbauer, V.; Krechmer, J.; Lehtipalo, K.; Lamkaddam, H.; Lampimäki, M.; Lee, C. P.; Makhmutov, V.; Marie, G.; Mathot, S.; Mauldin, R. L.; Mentler, B.; Müller, T.; Onnela, A.; Partoll, E.; Petäjä, T.; Philippov, M.; Pospisilova, V.; Ranjithkumar, A.; Rissanen, M.; Rörup, B.; Scholz, W.; Shen, J.; Simon, M.; Sipilä, M.; Steiner, G.; Stolzenburg, D.; Tham, Y. J.; Tomé, A.; Wagner, A. C.; Wang, D. S.; Wang, Y.; Weber, S. K.; Winkler, P. M.; Wlasits, P. J.; Wu, Y.; Xiao, M.; Ye, Q.; Zauner-Wieczorek, M.; Zhou, X.; Volkamer, R.; Riipinen, I.; Dommen, J.; Curtius, J.; Baltensperger, U.; Kulmala, M.; Worsnop, D. R.; Kirkby, J.; Seinfeld, J. H.; El-Haddad, I.; Flagan, R. C.; Donahue, N. M. Rapid Growth of New Atmospheric Particles by Nitric Acid and Ammonia Condensation. *Nature* **2020**, *581* (7807), 184−189.

(8) Deng, C.; Cai, R.; Yan, C.; Zheng, J.; Jiang, J. Formation and Growth of Sub-3 nm Particles in Megacities: Impact of Background Aerosols. *Faraday Discuss.* **2021**, *226* (0), 348−363.

(9) Kontkanen, J.; Lehtipalo, K.; Ahonen, L.; Kangasluoma, J.; Manninen, H. E.; Hakala, J.; Rose, C.; Sellegri, K.; Xiao, S.; Wang, L.; Qi, X.; Nie, W.; Ding, A.; Yu, H.; Lee, S.; Kerminen, V.-M.; Petäjä, T.; Kulmala, M. Measurements of Sub-3 nm Particles Using a Particle Size Magnifier in Different Environments: From Clean Mountain Top to Polluted Megacities. *Atmos. Chem. Phys.* **2017**, *17* (3), 2163−2187.

(10) Patra, S. S.; Liu, J.; Jiang, J.; Ding, X.; Huang, C.; Keech, C.; Steiner, G.; Stevens, P. S.; Jung, N.; Boor, B. E. Rapid Nucleation and

Growth of Indoor Atmospheric Nanocluster Aerosol during the Use of Scented Volatile Chemical Products in Residential Buildings. *ACS ES&T Air* **2024**, *1* (10), 1276−1293.
(11) Patra, S. S.; Jiang, J.; Liu, J.; Steiner, G.; Jung, N.; Boor, B. E. Flame-Free Candles Are Not Pollution-Free: Scented Wax Melts as a Significant Source of Atmospheric Nanoparticles. *Environ. Sci. Technol. Lett.* **2025**, *12* (2), 175−182.
(12) Tang, Q.; Cai, R.; You, X.; Jiang, J. Nascent Soot Particle Size Distributions down to 1 nm from a Laminar Premixed Burner-Stabilized Stagnation Ethylene Flame. *Proceedings of the Combustion Institute* **2017**, *36* (1), 993−1000.
(13) Wang, Y.; Fang, J.; Attoui, M.; Chadha, T. S.; Wang, W.-N.; Biswas, P. Application of Half Mini DMA for Sub 2 nm Particle Size Distribution Measurement in an Electrospray and a Flame Aerosol Reactor. *J. Aerosol Sci.* **2014**, *71*, 52−64.
(14) Carbone, F.; Attoui, M.; Gomez, A. Challenges of Measuring Nascent Soot in Flames as Evidenced by High-Resolution Differential Mobility Analysis. *Aerosol Sci. Technol.* **2016**, *50* (7), 740−757.
(15) Sgro, L. A.; D'Anna, A.; Minutolo, P. Charge Distribution of Incipient Flame-Generated Particles. *Aerosol Sci. Technol.* **2010**, *44* (8), 651−662.
(16) Sgro, L. A.; D'Anna, A.; Minutolo, P. Charge Fraction Distribution of Nucleation Mode Particles: New Insight on the Particle Formation Mechanism. *Combust. Flame* **2011**, *158* (7), 1418−1425.
(17) Abid, A. D.; Tolmachoff, E. D.; Phares, D. J.; Wang, H.; Liu, Y.; Laskin, A. Size Distribution and Morphology of Nascent Soot in Premixed Ethylene Flames with and without Benzene Doping. *Proceedings of the Combustion Institute* **2009**, *32* (1), 681−688.
(18) Biswas, P.; Wang, Y.; Attoui, M. Sub-2 nm Particle Measurement in High-Temperature Aerosol Reactors: A Review. *Curr. Opin. Chem. Eng.* **2018**, *21*, 60−66.
(19) Betrancourt, C.; Liu, F.; Desgroux, P.; Mercier, X.; Faccinetto, A.; Salamanca, M.; Ruwe, L.; Kohse-Hoinghaus, K.; Emmrich, D.; Beyer, A.; Golzhauser, A.; Tritscher, T. Investigation of the Size of the Incandescent Incipient Soot Particles in Premixed Sooting and Nucleation Flames of n-Butane Using LII, HIM, and 1 nm-SMPS. *Aerosol Sci. Technol.* **2017**, *51* (8), 916−935.
(20) Kangasluoma, J.; Kontkanen, J. On the Sources of Uncertainty in the Sub-3 nm Particle Concentration Measurement. *J. Aerosol Sci.* **2017**, *112*, 34−51.
(21) Kangasluoma, J.; Cai, R.; Jiang, J.; Deng, C.; Stolzenburg, D.; Ahonen, L. R.; Chan, T.; Fu, Y.; Kim, C.; Laurila, T. M.; Zhou, Y.; Dada, L.; Sulo, J.; Flagan, R. C.; Kulmala, M.; Petäjä, T.; Lehtipalo, K. Overview of Measurements and Current Instrumentation for 1−10 nm Aerosol Particle Number Size Distributions. *J. Aerosol Sci.* **2020**, *148*, No. 105584.
(22) Su, Z.; Zhou, W.; Zhang, Y. New Insight into the Soot Nanoparticles in a Candle Flame. *Chem. Commun.* **2011**, *47* (16), 4700−4702.
(23) Bekö, G.; Weschler, C. J.; Wierzbicka, A.; Karottki, D. G.; Toftum, J.; Loft, S.; Clausen, G. Ultrafine Particles: Exposure and Source Apportionment in 56 Danish Homes. *Environ. Sci. Technol.* **2013**, *47* (18), 10240−10248.
(24) Wallace, L.; Jeong, S.-G.; Rim, D. Dynamic Behavior of Indoor Ultrafine Particles (2.3−64 nm) Due to Burning Candles in a Residence. *Indoor Air* **2019**, *29* (6), 1018−1027.
(25) Rasmussen, B. B.; Wang, K.; Karstoft, J. G.; Skov, S. N.; Køcks, M.; Andersen, C.; Wierzbicka, A.; Pagels, J.; Pedersen, P. B.; Glasius, M.; Bilde, M. Emissions of Ultrafine Particles from Five Types of Candles during Steady Burn Conditions. *Indoor Air* **2021**, *31* (4), 1084−1094.
(26) Pedata, P.; Boccellino, M.; La Porta, R.; Napolitano, M.; Minutolo, P.; Sgro, L. A.; Zei, F.; Sannolo, N.; Quagliuolo, L. Interaction between Combustion-Generated Organic Nanoparticles and Biological Systems: In Vitro Study of Cell Toxicity and Apoptosis in Human Keratinocytes. *Nanotoxicology* **2012**, *6* (4), 338−352.
(27) Pedata, P.; Bergamasco, N.; D'Anna, A.; Minutolo, P.; Servillo, L.; Sannolo, N.; Balestrieri, M. L. Apoptotic and Proinflammatory Effect of Combustion-Generated Organic Nanoparticles in Endothelial Cells. *Toxicol. Lett.* **2013**, *219* (3), 307−314.
(28) Sgro, L. A.; Simonelli, A.; Pascarella, L.; Minutolo, P.; Guarnieri, D.; Sannolo, N.; Netti, P.; D'Anna, A. Toxicological Properties of Nanoparticles of Organic Compounds (NOC) from Flames and Vehicle Exhausts. *Environ. Sci. Technol.* **2009**, *43* (7), 2608−2613.
(29) Garcia, G. J. M.; Schroeter, J. D.; Kimbell, J. S. Olfactory Deposition of Inhaled Nanoparticles in Humans. *Inhal. Toxicol.* **2015**, *27* (8), 394−403.
(30) Peters, A.; Rückerl, R.; Cyrys, J. Lessons from Air Pollution Epidemiology for Studies of Engineered Nanomaterials. *J. Occup. Environ. Med.* **2011**, *53*, S8−S13.
(31) Kreyling, W. G.; Hirn, S.; Möller, W.; Schleh, C.; Wenk, A.; Celik, G.; Lipka, J.; Schäffler, M.; Haberl, N.; Johnston, B. D.; Sperling, R.; Schmid, G.; Simon, U.; Parak, W. J.; Semmler-Behnke, M. Air−Blood Barrier Translocation of Tracheally Instilled Gold Nanoparticles Inversely Depends on Particle Size. *ACS Nano* **2014**, *8* (1), 222−233.
(32) Oberdörster, G.; Sharp, Z.; Atudorei, V.; Elder, A.; Gelein, R.; Kreyling, W.; Cox, C. Translocation of Inhaled Ultrafine Particles to the Brain. *Inhal. Toxicol.* **2004**, *16* (6−7), 437−445.
(33) Faherty, T.; Raymond, J. E.; McFiggans, G.; Pope, F. D. Acute Particulate Matter Exposure Diminishes Executive Cognitive Functioning after Four Hours Regardless of Inhalation Pathway. *Nat. Commun.* **2025**, *16* (1), 1339.
(34) Steiner, G.; Flentje, H.; Väkevä, M.; Keck, L.; Vanhanen, J. Monitoring Ambient Aerosol Size Distributions from 1 - 55 nm with the GRIMM-AIRMODUS PSMPS. In *EGU General Assembly 2021*, 2021; p EGU21−12472.
(35) Kulmala, M.; Petäjä, T.; Nieminen, T.; Sipilä, M.; Manninen, H. E.; Lehtipalo, K.; Dal Maso, M.; Aalto, P. P.; Junninen, H.; Paasonen, P.; Riipinen, I.; Lehtinen, K. E. J.; Laaksonen, A.; Kerminen, V.-M. Measurement of the Nucleation of Atmospheric Aerosol Particles. *Nat. Protoc.* **2012**, *7* (9), 1651−1667.
(36) Cai, R.; Yang, D.; Fu, Y.; Wang, X.; Li, X.; Ma, Y.; Hao, J.; Zheng, J.; Jiang, J. Aerosol Surface Area Concentration: A Governing Factor in New Particle in Beijing. *Atmos. Chem. Phys.* **2017**, *17* (20), 12327−12340.
(37) Ding, X.; Jiang, J.; Shah, A. D.; Jung, N. Peracetic Acid Emissions and Exposures during Building Disinfection Events. *Build. Environ.* **2025**, *269*, No. 112221.
(38) Jiang, J.; Ding, X.; Patra, S. S.; Cross, J. N.; Huang, C.; Kumar, V.; Price, P.; Reidy, E. K.; Tasoglou, A.; Huber, H.; Stevens, P. S.; Boor, B. E.; Jung, N. Siloxane Emissions and Exposures during the Use of Hair Care Products in Buildings. *Environ. Sci. Technol.* **2023**, *57* (48), 19999−20009.
(39) Liu, J.; Jiang, J.; Patra, S. S.; Ding, X.; Huang, C.; Cross, J. N.; Magnuson, B. H.; Jung, N. Indoor Nanoparticle Emissions and Exposures during Heat-Based Hair Styling Activities. *Environ. Sci. Technol.* **2025**, *59* (32), 17103−17115.
(40) Patra, S. S.; Ramsisaria, R.; Du, R.; Wu, T.; Boor, B. E. A Machine Learning Field Calibration Method for Improving the Performance of Low-Cost Particle Sensors. *Build. Environ.* **2021**, *190*, No. 107457.
(41) Patra, S. S.; Wu, T.; Wagner, D. N.; Jiang, J.; Boor, B. E. Real-Time Measurements of Fluorescent Aerosol Particles in a Living Laboratory Office under Variable Human Occupancy and Ventilation Conditions. *Build. Environ.* **2021**, *205*, No. 108249.
(42) Perring, A. E.; Schwarz, J. P.; Baumgardner, D.; Hernandez, M. T.; Spracklen, D. V.; Heald, C. L.; Gao, R. S.; Kok, G.; McMeeking, G. R.; McQuaid, J. B.; Fahey, D. W. Airborne Observations of Regional Variation in Fluorescent Aerosol across the United States. *J. Geophys. Res.: Atmos.* **2015**, *120* (3), 1153−1170.
(43) Jiang, J.; Ding, X.; Tasoglou, A.; Huber, H.; Shah, A. D.; Jung, N.; Boor, B. E. Real-Time Measurements of Botanical Disinfectant Emissions, Transformations, and Multiphase Inhalation Exposures in Buildings. *Environ. Sci. Technol. Lett.* **2021**, *8* (7), 558−566.

(44) Jiang, J.; Ding, X.; Isaacson, K. P.; Tasoglou, A.; Huber, H.; Shah, A. D.; Jung, N.; Boor, B. E. Ethanol-Based Disinfectant Sprays Drive Rapid Changes in the Chemical Composition of Indoor Air in Residential Buildings. *J. Hazard. Mater. Lett.* **2021**, *2*, No. 100042.
(45) Saari, S.; Arffman, A.; Harra, J.; Rönkkö, T.; Keskinen, J. Performance Evaluation of the HR-ELPI+ Inversion. *Aerosol Sci. Technol.* **2018**, *52* (9), 1037−1047.
(46) Fonseca, A. S.; Viana, M.; Pérez, N.; Alastuey, A.; Querol, X.; Kaminski, H.; Todea, A. M.; Monz, C.; Asbach, C. Intercomparison of a Portable and Two Stationary Mobility Particle Sizers for Nanoscale Aerosol Measurements. *Aerosol Sci. Technol.* **2016**, *50* (7), 653−668.
(47) Vo, E.; Horvatin, M.; Zhuang, Z. Performance Comparison of Field Portable Instruments to the Scanning Mobility Particle Sizer Using Monodispersed and Polydispersed Sodium Chloride Aerosols. *Ann. Work Expo. Health* **2018**, *62* (6), 711−720.
(48) Hsiao, T.-C.; Lee, Y.-C.; Chen, K.-C.; Ye, W.-C.; Sopajaree, K.; Tsai, Y. I. Experimental Comparison of Two Portable and Real-Time Size Distribution Analyzers for Nano/Submicron Aerosol Measurements. *Aerosol Air Qual. Res.* **2016**, *16* (4), 919−929.
(49) Wu, T.; Boor, B. E. Characterization of a Thermal Aerosol Generator for HVAC Filtration Experiments (RP-1734). *Sci. Technol. Built Environ.* **2020**, *26* (6), 816−834.
(50) Pagels, J.; Wierzbicka, A.; Nilsson, E.; Isaxon, C.; Dahl, A.; Gudmundsson, A.; Swietlicki, E.; Bohgard, M. Chemical Composition and Mass Emission Factors of Candle Smoke Particles. *J. Aerosol Sci.* **2009**, *40* (3), 193−208.
(51) Lai, A. C. K.; Nazaroff, W. W. Modeling Indoor Particle Deposition from Turbulent Flow onto Smooth Surfaces. *J. Aerosol Sci.* **2000**, *31* (4), 463−476.
(52) Stolzenburg, D.; Cai, R.; Blichner, S. M.; Kontkanen, J.; Zhou, P.; Makkonen, R.; Kerminen, V.-M.; Kulmala, M.; Riipinen, I.; Kangasluoma, J. Atmospheric Nanoparticle Growth. *Rev. Mod. Phys.* **2023**, *95* (4), 45002.
(53) Cai, R.; Häkkinen, E.; Yan, C.; Jiang, J.; Kulmala, M.; Kangasluoma, J. The Effectiveness of the Coagulation Sink of 3−10 nm Atmospheric Particles. *Atmos. Chem. Phys.* **2022**, *22* (17), 11529−11541.
(54) De Falco, G.; Commodo, M.; Minutolo, P.; D'Anna, A. Flame-Formed Carbon Nanoparticles: Morphology, Interaction Forces, and Hamaker Constant from AFM. *Aerosol Sci. Technol.* **2015**, *49* (5), 281−289.
(55) Cai, R.; Jiang, J. A New Balance Formula to Estimate New Particle Formation Rate: Reevaluating Effect of Coagulation Scavenging. *Atmos. Chem. Phys.* **2017**, *17* (20), 12659−12675.
(56) Cai, R.; Li, C.; He, X.-C.; Deng, C.; Lu, Y.; Yin, R.; Yan, C.; Wang, L.; Jiang, J.; Kulmala, M.; Kangasluoma, J. Impacts of Coagulation on the Appearance Time Method for New Particle Growth Evaluation and Their Corrections. *Atmos. Chem. Phys.* **2021**, *21* (3), 2287−2304.
(57) Gong, Y.; Hu, M.; Cheng, Y.; Su, H.; Yue, D.; Liu, F.; Wiedensohler, A.; Wang, Z.; Kalesse, H.; Liu, S.; Wu, Z.; Xiao, K.; Mi, P.; Zhang, Y. Competition of Coagulation Sink and Source Rate: New Particle Formation in the Pearl River Delta of China. *Atmos. Environ.* **2010**, *44* (27), 3278−3285.
(58) Kuang, C.; Riipinen, I.; Sihto, S.-L.; Kulmala, M.; McCormick, A. V.; McMurry, P. H. An Improved Criterion for New Particle Formation in Diverse Atmospheric Environments. *Atmos. Chem. Phys.* **2010**, *10* (17), 8469−8480.
(59) McMurry, P. H.; Fink, M.; Sakurai, H.; Stolzenburg, M. R.; Mauldin, R. L.; Smith, J.; Eisele, F.; Moore, K.; Sjostedt, S.; Tanner, D.; Huey, L. G.; Nowak, J. B.; Edgerton, E.; Voisin, D. A Criterion for New Particle Formation in the Sulfur-Rich Atlanta Atmosphere. *J. Geophys. Res.: Atmos.* **2005**, *110* (D22), D22S02.
(60) Wu, T.; Täubel, M.; Holopainen, R.; Viitanen, A.-K.; Vainiotalo, S.; Tuomi, T.; Keskinen, J.; Hyvärinen, A.; Hämeri, K.; Saari, S. E.; Boor, B. E. Infant and Adult Inhalation Exposure to Resuspended Biological Particulate Matter. *Environ. Sci. Technol.* **2018**, *52* (1), 237−247.
(61) Roth, K. Chemistry of the Christmas Candle — Part 2. *ChemistryViews* **2011**, 424.
(62) Wang, H. Formation of Nascent Soot and Other Condensed-Phase Materials in Flames. *Proceedings of the Combustion Institute* **2011**, *33* (1), 41−67.
(63) Veshkini, A. *Understanding Soot Particle Growth Chemistry and Particle Sizing Using a Novel Soot Growth and Formation Model*; Ph.D. Thesis; University of Toronto: Canada, 2015.
(64) Sirignano, M.; Kent, J.; D'Anna, A. Further Experimental and Modelling Evidences of Soot Fragmentation in Flames. *Proceedings of the Combustion Institute* **2015**, *35* (2), 1779−1786.
(65) Echavarria, C. A.; Jaramillo, I. C.; Sarofim, A. F.; Lighty, J. S. Studies of Soot Oxidation and Fragmentation in a Two-Stage Burner under Fuel-Lean and Fuel-Rich Conditions. *Proceedings of the Combustion Institute* **2011**, *33* (1), 659−666.
(66) Maricq, M. M. Size and Charge of Soot Particles in Rich Premixed Ethylene Flames. *Combust. Flame* **2004**, *137* (3), 340−350.
(67) Botero, M. L.; Sheng, Y.; Akroyd, J.; Martin, J.; Dreyer, J. A. H.; Yang, W.; Kraft, M. Internal Structure of Soot Particles in a Diffusion Flame. *Carbon* **2019**, *141*, 635−642.
(68) Wang, H.; Guan, J.; Xu, G.; Mercier, X.; Zhang, J.; Guo, H.; Yu, T.; Gui, H.; Huang, T.; Truhlar, D. G.; Wang, Z. Resonance-Stabilized Radical Clustering Bridges the Gap between Gaseous Precursors and Soot in the Inception Stage. *Proc. Natl. Acad. Sci. U. S. A.* **2025**, *122* (18), No. e2503292122.
(69) Wang, K.; Rasmussen, B. B.; Thomsen, D.; Zhang, Y.; Jensen, M. M.; Kristensen, K.; Hoffmann, T.; Glasius, M.; Bilde, M. Influence of Candle Emissions on Monoterpene Oxidation Chemistry and Secondary Organic Aerosol. *Environ. Sci. Technol.* **2024**, *58* (48), 21265−21274.
(70) Heinritzi, M.; Dada, L.; Simon, M.; Stolzenburg, D.; Wagner, A. C.; Fischer, L.; Ahonen, L. R.; Amanatidis, S.; Baalbaki, R.; Baccarini, A.; Bauer, P. S.; Baumgartner, B.; Bianchi, F.; Brilke, S.; Chen, D.; Chiu, R.; Dias, A.; Dommen, J.; Duplissy, J.; Finkenzeller, H.; Frege, C.; Fuchs, C.; Garmash, O.; Gordon, H.; Granzin, M.; El Haddad, I.; He, X.; Helm, J.; Hofbauer, V.; Hoyle, C. R.; Kangasluoma, J.; Keber, T.; Kim, C.; Kürten, A.; Lamkaddam, H.; Laurila, T. M.; Lampilahti, J.; Lee, C. P.; Lehtipalo, K.; Leiminger, M.; Mai, H.; Makhmutov, V.; Manninen, H. E.; Marten, R.; Mathot, S.; Mauldin, R. L.; Mentler, B.; Molteni, U.; Müller, T.; Nie, W.; Nieminen, T.; Onnela, A.; Partoll, E.; Passananti, M.; Petäjä, T.; Pfeifer, J.; Pospisilova, V.; Quéléver, L. L. J.; Rissanen, M. P.; Rose, C.; Schobesberger, S.; Scholz, W.; Scholze, K.; Sipilä, M.; Steiner, G.; Stozhkov, Y.; Tauber, C.; Tham, Y. J.; Vazquez-Pufleau, M.; Virtanen, A.; Vogel, A. L.; Volkamer, R.; Wagner, R.; Wang, M.; Weitz, L.; Wimmer, D.; Xiao, M.; Yan, C.; Ye, P.; Zha, Q.; Zhou, X.; Amorim, A.; Baltensperger, U.; Hansel, A.; Kulmala, M.; Tomé, A.; Winkler, P. M.; Worsnop, D. R.; Donahue, N. M.; Kirkby, J.; Curtius, J. Molecular Understanding of the Suppression of New-Particle Formation by Isoprene. *Atmos. Chem. Phys.* **2020**, *20* (20), 11809−11821.
(71) Liu, J.; Jiang, J.; Ding, X.; Patra, S. S.; Cross, J. N.; Huang, C.; Kumar, V.; Price, P.; Reidy, E. K.; Tasoglou, A.; Huber, H.; Stevens, P. S.; Boor, B. E.; Jung, N. Real-Time Evaluation of Terpene Emissions and Exposures during the Use of Scented Wax Products in Residential Buildings with PTR-TOF-MS. *Build. Environ.* **2024**, *255*, No. 111314.
(72) Seinfeld, J. H.; Pandis, S. N. *Atmospheric Chemistry and Physics: From Air Pollution to Climate Change*; John Wiley & Sons, 2016.
(73) Reichman, R.; Shirazi, E.; Colliver, D. G.; Pennell, K. G. US Residential Building Air Exchange Rates: New Perspectives to Improve Decision Making at Vapor Intrusion Sites. *Environ. Sci.: Processes Impacts* **2017**, *19* (2), 87−100.
(74) Lee, W.-C.; Wolfson, J. M.; Catalano, P. J.; Rudnick, S. N.; Koutrakis, P. Size-Resolved Deposition Rates for Ultrafine and Submicrometer Particles in a Residential Housing Unit. *Environ. Sci. Technol.* **2014**, *48* (17), 10282−10290.
(75) Winkler, P. M.; Vrtala, A.; Wagner, P. E. The Role of Ions in Condensation Particle Counting for Particle Diameters Below 2 nm.

https://doi.org/10.1021/acs.est.5c05577
Environ. Sci. Technol. 2026, 60, 834−846

In *Nucleation and Atmospheric Aerosols*; O'Dowd, C. D., Wagner, P. E., Eds.; Springer, Netherlands: Dordrecht, 2007; pp 73−77.
(76) Olenius, T.; Roldin, P. Role of Gas−Molecular Cluster−Aerosol Dynamics in Atmospheric New-Particle Formation. *Sci. Rep.* **2022**, *12* (1), 10135.
(77) Ehn, M.; Thornton, J. A.; Kleist, E.; Sipilä, M.; Junninen, H.; Pullinen, I.; Springer, M.; Rubach, F.; Tillmann, R.; Lee, B.; Lopez-Hilfiker, F.; Andres, S.; Acir, I.-H.; Rissanen, M.; Jokinen, T.; Schobesberger, S.; Kangasluoma, J.; Kontkanen, J.; Nieminen, T.; Kurtén, T.; Nielsen, L. B.; Jørgensen, S.; Kjaergaard, H. G.; Canagaratna, M.; Maso, M. D.; Berndt, T.; Petäjä, T.; Wahner, A.; Kerminen, V.-M.; Kulmala, M.; Worsnop, D. R.; Wildt, J.; Mentel, T. F. A Large Source of Low-Volatility Secondary Organic Aerosol. *Nature* **2014**, *506* (7489), 476−479.
(78) Sulo, J.; Sarnela, N.; Kontkanen, J.; Ahonen, L.; Paasonen, P.; Laurila, T.; Jokinen, T.; Kangasluoma, J.; Junninen, H.; Sipilä, M.; Petäjä, T.; Kulmala, M.; Lehtipalo, K. Long-Term Measurement of Sub-3 nm Particles and Their Precursor Gases in the Boreal Forest. *Atmos. Chem. Phys.* **2021**, *21* (2), 695−715.
(79) Perraud, V.; Li, X.; Jiang, J.; Finlayson-Pitts, B. J.; Smith, J. N. Size-Resolved Chemical Composition of Sub-20 nm Particles from Methanesulfonic Acid Reactions with Methylamine and Ammonia. *ACS Earth Space Chem.* **2020**, *4* (7), 1182−1194.
(80) Zhang, K.; Xu, Z.; Gao, J.; Xu, Z.; Wang, Z. Review of Online Measurement Techniques for Chemical Composition of Atmospheric Clusters and Sub-20 nm Particles. *Front. Environ. Sci.* **2022**, *10*, 937006.

https://doi.org/10.1021/acs.est.5c05577
Environ. Sci. Technol. 2026, 60, 834−846